ADVANCING EARTH AND SPACE SCIENCES

Geophysical Research Letters

RESEARCH LETTER
10.1029/2026GL125630

Land Radiative Management Increases Heat Stress in Some Humid Regions

Yu Cheng[1,2] and Kaighin A. McColl[2,3]

[1]Shanghai Key Laboratory of Ocean-land-atmosphere Boundary Dynamics and Climate Change, Department of Atmospheric and Oceanic Sciences, Fudan University, Shanghai, China, [2]Department of Earth and Planetary Sciences, Harvard University, Cambridge, MA, USA, [3]School of Engineering and Applied Sciences, Harvard University, Cambridge, MA, USA

Key Points:

- Land radiative management can increase wet-bulb temperatures in surrounding humid regions
- The insensitivity of relative humidity to soil drying causes wet-bulb temperatures to rise with warming in sufficiently humid climates
- LRM may exacerbate heat stress in hot and humid regions despite its intended cooling effects

Supporting Information:

Supporting Information may be found in the online version of this article.

Correspondence to:

K. A. McColl,
kmccoll@seas.harvard.edu

Citation:

Cheng, Y., & McColl, K. A. (2026). Land radiative management increases heat stress in some humid regions. *Geophysical Research Letters*, *53*, e2026GL125630. https://doi.org/10.1029/2026GL125630

Received 21 JUL 2026
Accepted 20 AUG 2026

Abstract Heat stress may exceed human physiological limits this century in hot and humid regions. Land radiative management (LRM), a geoengineering strategy that increases surface albedo, aims to reduce heat stress. However, previous work has shown that LRM suppresses rainfall in surrounding regions, drying soils and increasing temperatures. Because soil drying typically reduces wet-bulb temperatures, a key heat stress metric, one might expect heat stress to decline. Here, we use cloud-permitting simulations to show that, in sufficiently humid climates, LRM causes wet-bulb temperatures to rise in surrounding regions, even as soils dry. This occurs because relative humidity in humid regions is largely insensitive to soil drying, resulting in increasing wet-bulb temperatures with warming. In drier climates, soil drying reduces relative humidity and wet-bulb temperatures, consistent with prior studies. While hot and humid regions might seem ideal for LRM, it may ultimately increase heat stress.

Plain Language Summary Land radiative management (LRM)—increasing land reflectivity to reduce regional warming—has been proposed as a geoengineering strategy. Combining high resolution simulations and a simple theory, we show that in hot and humid regions, LRM can unexpectedly increase, rather than decrease, human heat stress in surrounding regions. By amplifying heat stress in neighboring regions, LRM may inadvertently worsen heat inequality, particularly in hot and humid areas such as South and Southwest Asia, where LRM is most needed and population density is high.

1. Introduction

As temperatures rise due to greenhouse warming, heat stress will become an increasingly acute problem (Freychet et al., 2022). However, the heat stress exerted on the human body does not only depend on air temperature. Among other factors, humidity plays an important role, with higher humidity resulting in higher heat stress, all else equal (Buzan & Huber, 2020; Sherwood & Huber, 2010). This leads to some counter-intuitive results. For example, in some cases, cities may experience less heat stress compared to surrounding rural areas, even though near-surface air temperatures are typically higher in cities (Zhang et al., 2023). The wet-bulb temperature—a combined measure of heat and humidity—is widely used as a proxy for heat stress (Im et al., 2017; Raymond et al., 2020; Sherwood & Huber, 2010; Zhang et al., 2023). Hot and humid conditions imply high wet-bulb temperatures and high heat stress. In hot and humid regions such as south Asia (Im et al., 2017; Saeed et al., 2021), southwest Asia (Pal & Eltahir, 2016; Safieddine et al., 2022), and the southeastern United States (Powis et al., 2023), wet-bulb temperatures are projected to exceed critical thresholds (Fan & McColl, 2024; Sherwood & Huber, 2010; Vanos et al., 2023), potentially surpassing the limits of human physiological tolerance this century. Accordingly, urgent mitigation measures (Saeed et al., 2021; Safieddine et al., 2022; Vecellio et al., 2023) are needed to alleviate extreme heat stress in a warming world.

Among various mitigation strategies, land radiative management (LRM) has gained increasing attention (Jia et al., 2019; Seneviratne et al., 2018). LRM aims to decrease temperatures at local and regional scales by deliberately increasing surface albedo and, therefore, decreasing absorbed shortwave radiation at the land surface. Some proposed approaches to LRM include no-till farming (Davin et al., 2014; Seneviratne et al., 2018; Wilhelm et al., 2015), desert albedo enhancement (Irvine et al., 2011), and white roofs (Li et al., 2014; Mackey et al., 2012; Sharma et al., 2016; Vahmani et al., 2016) and pavements (Erell et al., 2014; Taleghani et al., 2016). LRM has been shown to reduce both mean (Irvine et al., 2011; Seneviratne et al., 2018) and extreme temperatures (Wilhelm et al., 2015), as intended.

However, LRM can also have severe unintended consequences. At mesoscales (O(10km)), Cheng and McColl (2024b) showed that LRM can cause temperatures to increase unexpectedly in surrounding regions, due to changes in precipitation and soil saturation driven by mesoscale storm formation mechanisms (Cheng et al., 2023; Wang et al., 2000). Given the growing attention to LRM (Jia et al., 2019; Seneviratne et al., 2018), it is essential to understand the impact of LRM on heat stress before it is implemented, especially in hot and humid regions where heat stress is already severe, and where LRM is most likely to be adopted. While prior work has focused on unintended impacts on temperature (Cheng & McColl, 2024b), it remains unclear if there are similar unintended impacts on humidity and, therefore, human heat stress. Indeed, recent work suggests that drier soils ultimately reduce heat stress by reducing humidity, even though they increase air temperatures (Kong & Huber, 2023; Wouters et al., 2022). Since the warming identified in a previous LRM study (Cheng & McColl, 2024b) is caused by drying soils, it might seem that the ultimate impact of LRM on heat stress is to reduce it.

Here, we use cloud-permitting simulations to show that, in some hot and humid climates, LRM does, in fact, increase heat stress in surrounding regions. More specifically, we use cloud-permitting simulations to investigate how changes in temperature and humidity caused by LRM impact wet-bulb temperatures for a range of climates, from humid to dry (we refer to regions with high relative humidity as "humid" in this study). In our simulations, an LRM region with higher surface albedo is prescribed at the center of an otherwise uniform idealized land surface (Figure S1 in Supporting Information S1). Our simulations are deliberately idealized. This permits a clearer understanding of the most important physical mechanisms, which strengthens the evidence for our findings, albeit at the cost of reduced realism. Understanding the impacts of implementing LRM in a particular place would require simulations specific to that location, although the mechanisms identified in our simulations will be relevant to many cases beyond those simulated here.

2. Methods

2.1. Wet-Bulb Temperature

If an air parcel is cooled at constant pressure by evaporation until it reaches saturation, the resulting temperature is called the wet-bulb temperature. More precisely, the wet-bulb temperature is defined by the implicit equation (e.g., X. Lee, 2018)

$$T_w + \frac{e^*(T_w)}{\gamma} = T_a + \frac{e^*(T_a)\,RH}{\gamma}, \tag{1}$$

where $e^*(T)$ is the saturation vapor pressure at temperature T, $\gamma \equiv \frac{c_p P}{\epsilon \lambda}$ is the psychrometric constant, c_p is the specific heat capacity of air at constant pressure, P is near-surface atmospheric pressure, ϵ is the ratio of molecular weights of water vapor and dry air, λ is the latent heat of vapourization, and RH is the near-surface relative humidity. Note that this differs from the wet-bulb globe temperature (WBGT), which also depends on radiation and wind (Budd, 2008).

In our calculations, we use the Magnus form approximation of the Clausius-Clapeyron relation for saturation vapor pressure:

$$e^*(T) = 610.94 \times e^{\frac{17.625(T-273.15)}{T-30.11}}, \tag{2}$$

where T is temperature (K).

2.2. Cloud-Permitting Simulations

We use the System for Atmospheric Modeling (SAM version 6.11.8; Khairoutdinov and Randall, 2003) to simulate the impact of a high albedo anomaly (an idealized LRM region) on an idealized land surface (Figure S1 in Supporting Information S1). The simulations used here include those in Cheng and McColl (2024b), with several additions. The cloud-permitting atmospheric model is coupled with a simplified land model (SLM; J. M. Lee and Khairoutdinov, 2015). Homogeneous bare soil is prescribed as the default land cover type, although we perform additional simulations in which land cover type is varied (grassland and urban). We include a diurnal cycle, but not a seasonal cycle; instead, we repeat the insolation for January 1 for approximately 1,000 days to reach a quasi-equilibrium state (Table S1 in Supporting Information S1). In our analyses, we report 6 a.m.–6 p.m. averages, relevant to daytime heat stress. Longwave and shortwave radiation are computed using the National Center for Atmospheric Research (NCAR) Community Climate Model (CCM3) radiative transfer scheme (Kiehl et al., 1998). Subgrid-scale (SGS) turbulent fluxes are computed with a prognostic turbulent kinetic energy budget model using a 1.5-order closure scheme (Khairoutdinov & Randall, 2003). The mixing ratios of hydrometeor species are computed using the single-moment SAM1MOM scheme (Khairoutdinov & Randall, 2003). Our baseline simulations are run in radiative-convective equilibrium (RCE; Manabe and Strickler, 1964; Manabe and Wetherald, 1967), an idealized state in which radiative cooling exactly balances convective heating, although we conduct additional experiments that relax this approximation (see below). While commonly used as an approximation of the tropics, recent work has shown that RCE is a surprisingly reasonable approximation of the climatology of midlatitude land surfaces (Matthews et al., 2026; Miyawaki et al., 2022). Our baseline simulations incorporate an idealized land surface with no ocean, and no external moisture source. Instead, moisture is entirely recycled between land and atmosphere, with no moisture flux convergence from outside the modeled domain. While idealized, this is a reasonable approximation of many inland continental regions (see, e.g., Figure S2 of Dagan and Stier (2020); or Figure 3 of Van der Ent et al. (2010)). We also conduct further experiments that incorporate an external moisture source (described below).

We prescribe a high surface albedo anomaly at the center of the modeled domain to represent the LRM region (Figure S1 in Supporting Information S1). Since surface albedo varies with soil moisture, we prescribe dry surface values, and report both visible and near-infrared (NIR) values for all simulations in Table S1 in Supporting Information S1. Relative to the background region, we increase both the visible and NIR albedos by an equivalent percentage in the LRM region. We chose a constant albedo contrast between the LRM and background regions that is consistent with prior literature on the topic (Davin et al., 2014), while acknowledging that the contrast would vary considerably in practice based on implementation details. Two exceptions to these rules are the simulations in which land cover was varied (discussed further below), for which we applied different fractional increases to the visible and NIR albedos in the LRM region, to test sensitivity to the NIR-weighting of the surface albedo modification. Those simulations also include a lower broadband surface albedo contrast between the LRM and background regions, to allow examination of the sensitivity of our findings to varying this quantity.

Our simulations span a wide range of climates, from dry to humid. Top-of-atmosphere insolation is varied (Table S1 in Supporting Information S1), leading to a wide range of daytime-averaged near-surface air temperatures (Table S2 in Supporting Information S1). The relative humidity in each simulation naturally varies in response to prescribed insolation, with warmer simulations typically leading to lower relative humidity and soil moisture (the A_RCE simulations in Tables S1 and S2 in Supporting Information S1). To sample climates that are both hot and humid, we run an additional set of simulations, where soil saturation is nudged to relatively high values (A_RCE_nudgesoil), over a 24-hr time scale, keeping soil saturation within a narrow range (0.27–0.29; Tables S1 and S2 in Supporting Information S1). This results in simulations with high soil saturation, on average, while still allowing the land surface to interact with the atmosphere. This leads to soil saturation profiles with a similar spatial structure to those in simulations where soil saturation is not nudged. For example, in the nudged simulations, soil saturation is still typically lower over the LRM region, and a discontinuity forms at the boundary between the LRM region and its surroundings, as documented in Cheng and McColl (2024b).

Several additional simulations are performed to evaluate the sensitivity of our results to various modeling choices. First, we include a simulation with a mean wind (A_RCE_wind, Table S1 in Supporting Information S1). The mean wind is prescribed with velocity $U = 10$ m s^{-1} (in the x direction) at heights above 400 m. Below 400 m, the prescribed mean wind is linearly reduced to 0 m s^{-1} at the surface. Second, rather than assuming RCE, we parameterize the large-scale atmospheric forcing using the weak temperature gradient approximation (WTG, Sobel et al., 2001), a common approximation of tropical atmospheric dynamics (A_WTG, Table S1 in Supporting Information S1). We use the reference temperature profile from Abbott and Cronin (2021). Third, we vary the size of the domain and the geometry of the LRM region (Figure S1 in Supporting Information S1; B_WTG, Table S1 in Supporting Information S1). Fourth, we vary the land cover type (grassland and urban) using a configuration that is otherwise identical to the simulation A_RCE (A_RCE_grassland and A_RCE_urban; Table S1 in Supporting Information S1). Fifth, we include an external moisture source by splitting the domain equally between land and ocean (C_RCE, Table S1 and Figure S1 in Supporting Information S1).

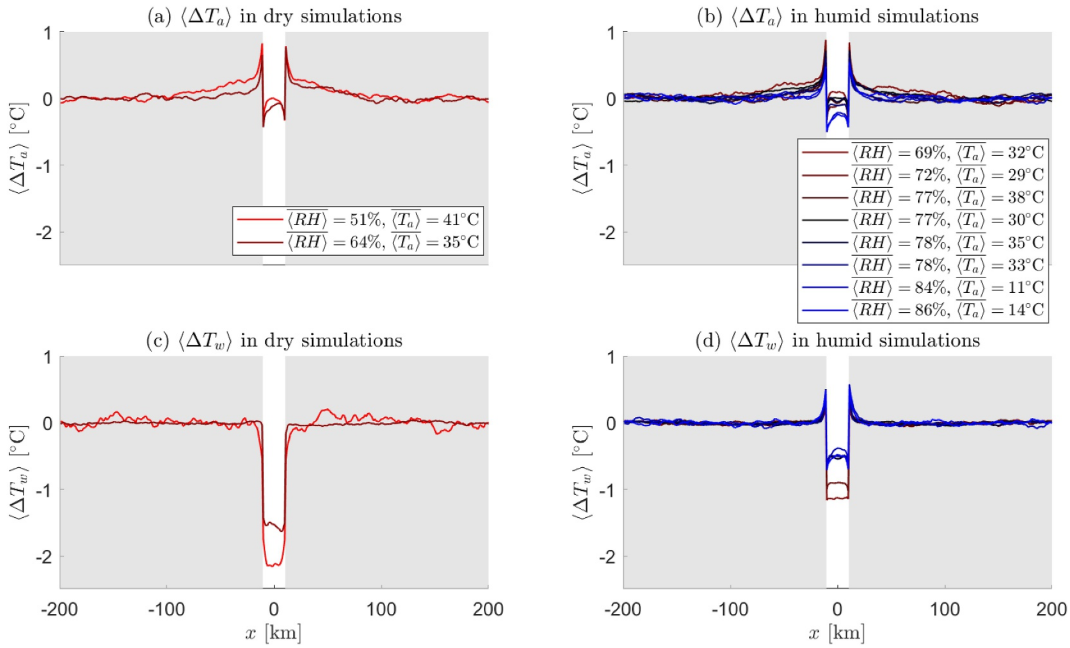

Figure 1. LRM causes higher wet-bulb temperatures in nearby surrounding regions, but only in humid climates. (a) and (b) Near-surface air temperature anomalies ($\langle \Delta T_a \rangle \equiv \langle T_a \rangle - T_{a_0}$), where T_a is near-surface air temperature (2 m above the surface) averaged between 6 a.m. and 6 p.m. from experiments A_RCE and A_RCE_nudgesoil (Table S1 in Supporting Information S1), T_{a_0} is average near-surface air temperature far from the LRM region (and similarly for other terms with a "0" subscript), $\langle \cdot \rangle$ denotes long-term temporal averaging, and $\bar{\cdot}$ denotes spatial averaging over the domain. The LRM region is at the center of the domain (white, centered at $x = 0$), while the surrounding regions are shaded gray. See "Methods: Cloud-permitting simulations" for further details. (c) and (d) Same as (a) and (b), but for wet-bulb temperature T_w. (a) and (c) correspond to simulations of dry climates with low average near-surface relative humidity ($\overline{\langle RH \rangle}$). (b) and (d) correspond to humid climates.

2.3. Decomposition of Wet-Bulb Temperature

This section derives the wet-bulb temperature decomposition used in Figure 2 and Figure S4 in Supporting Information S1. The difference in T_w between two different regions can be written as

$$\Delta T_w + \frac{1}{\gamma}\frac{de^*}{dT}\bigg|_{T=T_w}\Delta T_w = \Delta T_a + \frac{1}{\gamma}\left(RH\frac{de^*}{dT}\bigg|_{T=T_a}\Delta T_a + e^*(T_a)\Delta RH\right), \tag{3}$$

where we have used Equation 1, and the approximation $\Delta e^*(T) \approx \frac{de^*(T)}{dT}\Delta T$. In the context of our simulations, ΔT_w is the difference between the time-averaged wet-bulb temperature and the time- and space-averaged wet-bulb temperature far from the LRM region. A region is regarded as "far" from the LRM region if it is at least 90 km away from it. Our results are not particularly sensitive to reasonable variations in the chosen distance threshold. Rearranging yields

$$\Delta T_w = \underbrace{\left(\frac{1 + \frac{1}{\gamma}\frac{de^*}{dT}\big|_{T=T_a} RH}{1 + \frac{1}{\gamma}\frac{de^*}{dT}\big|_{T=T_w}}\right)\Delta T_a}_{\text{Contributions from } T_a} + \underbrace{\left(\frac{\frac{1}{\gamma}e^*(T_a)}{1 + \frac{1}{\gamma}\frac{de^*}{dT}\big|_{T=T_w}}\right)\Delta RH}_{\text{Contributions from } RH}. \tag{4}$$

This decomposes ΔT_w into a contribution from differences in near-surface air temperature, and a contribution from differences in relative humidity. This decomposition accurately reproduces simulated ΔT_w with a root mean squared error (RMSE) of 0.026 K (Figure 2).

10.1029/2026GL125630

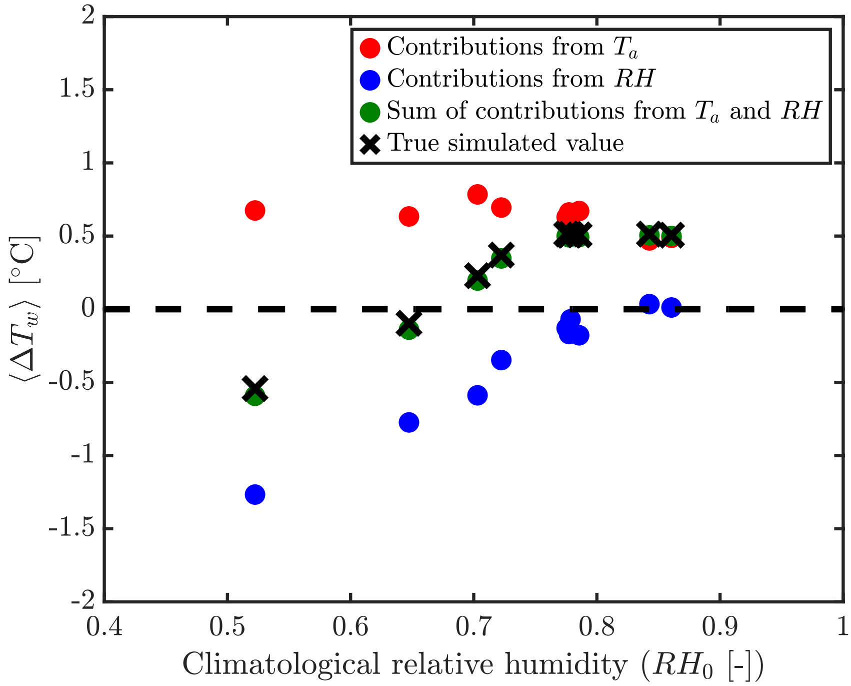

Figure 2. In dry climates, lower relative humidity reduces wet-bulb temperatures in the LRM region's immediate surroundings, but not in humid climates. Here, ΔT_w in the immediate surroundings of the LRM region is decomposed into contributions from near-surface air temperature and relative humidity. The decomposition accurately reproduces the simulated ΔT_w. See "Methods: Decomposition of wet-bulb temperature" for further details.

3. Results and Discussion

3.1. LRM Increases Air Temperatures in Surrounding Regions

As expected, near-surface air temperatures are typically lowest over the LRM region. Perhaps surprisingly, however, temperatures peak in the immediate surroundings of the LRM region (Figures 1a and 1b), and are higher than they would be in the absence of LRM. A mechanism was provided for this warming in a previous study (Cheng & McColl, 2024b), which we briefly summarize here. Inside the LRM region, temperatures decrease due to reductions in absorbed solar radiation, as expected. At the boundaries of the LRM region, mesoscale circulations form, driven by differential heating. The circulations reduce precipitation and soil saturation inside the LRM region. Precipitation and soil moisture are also reduced just outside the LRM region (Figure S2 in Supporting Information S1), in a region O(1 km) wide, which also reduces evaporative cooling. That region experiences the downsides of LRM (reduced evaporative cooling) without the upsides (reduced surface shortwave absorption). This results in warming just outside the LRM region.

3.2. LRM Increases Wet-Bulb Temperatures in Surrounding Regions, but Only for Humid Climates

In dry climates, LRM decreases wet-bulb temperatures in its immediate surroundings (Figure 1c), even though it increases air temperatures (Figure 1a). To understand why, we decompose the wet-bulb temperature anomaly into two components (Equation 4): one related to temperature, and the other related to relative humidity. For all climates, LRM causes warming in surrounding regions, which increases wet-bulb temperatures, absent other changes (red circles, Figure 2). However, LRM also reduces relative humidity in surrounding regions (Figure S3 in Supporting Information S1), which reduces wet-bulb temperatures, absent other changes (blue circles, Figure 2). In dry climates, reductions in wet-bulb temperature driven by relative humidity are large, leading to an overall reduction in wet-bulb temperatures (black crosses, Figure 2; Figure S4 in Supporting Information S1), despite increases from higher temperatures.

In contrast, in humid climates, reductions in wet-bulb temperature driven by relative humidity are small in the LRM region's immediate surroundings (blue circles, Figure 2; Figure S4 in Supporting Information S1), leading

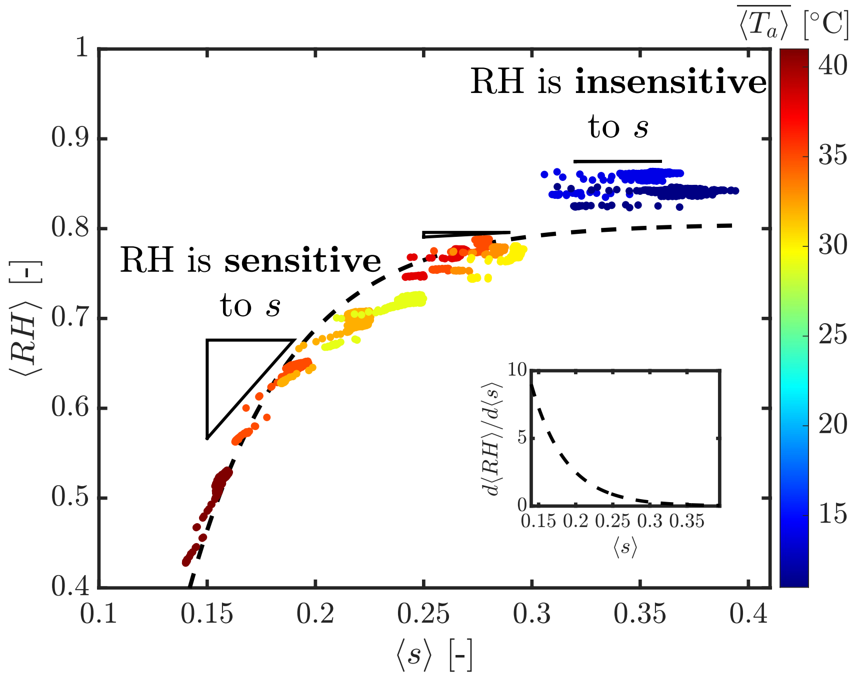

Figure 3. Relative humidity is sensitive to soil drying in dry climates, but not in humid climates. Each dot represents the long-term temporal average at a simulated grid point along the x-axis (averaged along the y-axis). Since there are 400 grid points in the x direction, each simulation contains 400 dots. The dashed curve is a fitted relationship between $\langle RH \rangle$ and $\langle s \rangle$, illustrating that relative humidity remains approximately insensitive to soil saturation in humid climates. The inset figure shows the gradient $\frac{d\langle RH \rangle}{d\langle s \rangle}$ as a function of $\langle s \rangle$. Other terms are defined as in Figure 1.

to an overall increase in wet-bulb temperatures (black crosses, Figures 2; Figure 1d), caused by increasing temperatures.

Why does LRM cause only minor changes in relative humidity in its immediate surroundings in humid climates, but not in dry climates? The relation between relative humidity and soil moisture is nonlinear (Figure 3). In humid climates, relative humidity is essentially insensitive to incremental reductions in soil moisture. This remains true even if the colder simulations ($\overline{\langle T_a \rangle} < 20$°C) are removed from Figure 3 (Figure S11 in Supporting Information S1). Therefore, in humid climates, reductions in soil moisture in surrounding regions caused by LRM have little impact on relative humidity. In contrast, in dry climates, relative humidity is quite sensitive to reductions in soil moisture. Accordingly, reductions in soil moisture in surrounding regions caused by LRM have a greater impact on relative humidity in dry climates.

The nonlinear relation between relative humidity and soil moisture can be understood more generally, beyond our simulations. First, over land, relative humidity is an approximately linear increasing function of the evaporative fraction (EF, the ratio of the latent heat flux to the sum of the surface turbulent fluxes; Betts (2000); McColl and Rigden (2020); McColl and Tang (2024)). Second, there is a well-known nonlinear relation between soil moisture and the evaporative fraction (Seneviratne et al., 2010). For dry soils, evaporation is "water limited," and the evaporative fraction increases with increasing soil moisture. For sufficiently wet soils, evaporation is "energy limited," and the evaporative fraction is essentially insensitive to increasing soil moisture. Combining these two results implies a nonlinear relation between soil moisture and relative humidity, similar to that shown in Figure 3.

This mechanism is robust to a wide range of changes. We found qualitatively similar results in simulations prescribed with the following modifications (Table S1 in Supporting Information S1): (a) adding a steady background wind, which shifted the warming pattern downwind (Figure S5 in Supporting Information S1); (b) using a simplified model of tropical large-scale dynamics, the weak temperature gradient (WTG) approximation (Sobel et al. (2001); Figure S6 in Supporting Information S1); (c) using a smaller domain, a reduced LRM area, and finer spatial resolution (Figure S7 in Supporting Information S1); (d) varying the land cover type, from grassland (Figure S8 in Supporting Information S1) to urban (Figure S9 in Supporting Information S1); and (e) incorporating an external moisture source (Figure S10 in Supporting Information S1). All of these simulations showed increases in wet-bulb temperatures in the imposed LRM region's immediate surroundings, so long as the simulated climate was sufficiently humid (Table S2 in Supporting Information S1). With sufficiently strong winds, we expect our mechanism would fail. However, the tropics are hot and humid, and are often modeled using similar assumptions to those made here, so we expect our core finding will apply to at least some hot and humid regions on Earth.

To summarize, LRM decreases precipitation both locally and in its immediate surroundings. This decreases soil moisture and increases air temperatures in the LRM region's immediate surroundings. In humid climates, where relative humidity is approximately invariant to changes in soil moisture, higher temperatures imply higher humidity and higher wet-bulb temperatures in the LRM region's immediate surroundings. This is not true of drier climates, where compensating declines in relative humidity counteract changes in wet-bulb temperatures.

3.3. Relation to Previous Studies

Previous studies investigated the influence of land-use change on temperature and wet-bulb temperature, focusing on irrigation (e.g., Krakauer et al., 2020), deforestation and afforestation (e.g., Alves de Oliveira et al., 2021), and urbanization (e.g., Yang et al., 2019). While interesting, those land-use changes are poor analogs to LRM, since they involve additional changes to surface roughness and heat capacity, beyond those made to albedo. Our simulations isolate the specific mechanisms relevant to LRM, in which only surface albedo is modified, by design.

Of the studies that have focused specifically on LRM, impacts on temperature have been evaluated at micrometeorological (Taleghani et al., 2016), regional (Davin et al., 2014), and global scales (Irvine et al., 2011; Wilhelm et al., 2015), but few studies have examined its effects on wet-bulb temperature and associated heat stress. In addition, as reviewed in Cheng and McColl (2024b), simulations conducted in previous studies on LRM suffer limitations that preclude them from reproducing the mechanism identified here. Those limitations include (a) an insufficiently fine model spatial resolution ($O(10\,\text{km})$), which fails to resolve mesoscale circulations (Davin et al., 2014; Irvine et al., 2011; Wilhelm et al., 2015); (b) an insufficiently large computational domain, which prevents mesoscale circulations from forming (Taleghani et al., 2016); (c) an insufficiently long averaging time period (no more than a few months), which prevents distinguishing the warming signal from the large internal variability in the hydrological cycle (Li et al., 2014; Sharma et al., 2016; Vahmani et al., 2016).

Beyond LRM, prior studies have typically found that dry soils reduce wet-bulb temperatures (Wouters et al., 2022), whereas wet soils increase them (Chagnaud et al., 2025; Kong & Huber, 2023). This mechanism agrees with our findings for drier climates, where decreasing soil saturation decreases humidity and wet-bulb temperatures. However, for humid climates, we find that relative humidity and wet-bulb temperatures are essentially invariant to changes in soil moisture (Figure 3), which may appear to conflict with prior studies. In fact, this result is consistent with prior studies (see, e.g., Figure 7 in Kong and Huber (2023)), although those studies tend to focus more on dry rather than humid conditions, where the sensitivity to soil moisture is greatest.

3.4. Limitations

Our analysis is subject to several limitations, beyond those already discussed. The mechanism we identify requires that soil moisture is sensitive to precipitation. We might expect this sensitivity to be weaker in urban areas where precipitation flows quickly over paved surfaces into drainage systems rather than soil reservoirs. To the extent that is true, it would reduce increases in both air temperature and humidity in the LRM region's immediate surroundings.

Our simulations do not incorporate hyperspectral radiative transfer, which can lead to errors in simulated surface albedo (Braghiere et al., 2023). However, they are unlikely to qualitatively impact our mechanism, even if the simulated surface shortwave absorption is somewhat quantitatively inaccurate. To the extent that the LRM scheme's increased surface albedo causes significant local cooling, as intended, a heating differential will arise and, at sufficiently large scales, mesoscale circulations will form and lead to warming near the boundaries, based on well-established physical mechanisms.

The proposed mechanism cannot currently be tested with observations, as LRM has not yet been implemented at mesoscales. Although natural albedo gradients exist, such as between cities and farmland, they are confounded by differences in surface roughness and vegetation, which substantially influence the heating contrast (Cheng & McColl, 2023). Nonetheless, the underlying mechanism is supported by fundamental physical principles and is robust to varying many aspects of the simulations.

Finally, wet-bulb temperature is not a complete measure of heat stress, which also depends on other quantities, including radiation, wind speed, and an individual's overall health (Fan & McColl, 2024; Vanos et al., 2023). However, there is overwhelming evidence that high wet-bulb temperatures are dangerous to human health (Fan & McColl, 2024; Sherwood & Huber, 2010; Vecellio et al., 2023).

3.5. Implications

We have shown that LRM can cause increases in wet-bulb temperatures in its immediate surroundings, so long as the climate is sufficiently humid. How important are those increases? They are large: in our simulations, they are consistently comparable to, or greater than, the reductions in wet-bulb temperature achieved inside the LRM region (Figure 1). Presumably, any declines in wet-bulb temperature inside the LRM region would need to be judged sufficiently important to justify the implementation of LRM in the first place. In that light, increases in wet-bulb temperature in surrounding regions of even larger magnitude are a major problem.

How many people would be impacted? Warming occurs in a relatively narrow band surrounding the LRM region. The width of this band is $O(1\text{ km})$, corresponding to the length scale over which precipitation transitions from lower values in the LRM region to higher values outside the LRM region (Cheng & McColl, 2024b). Despite the relatively small size of the region impacted, the number of people impacted could be large, both in absolute and relative terms. Consider an example, in which LRM is implemented over a 10 km × 10 km area, with warming extending 1 km beyond its boundaries. In absolute terms, for a population density similar to Mumbai's (~25,000 people/km^2; Government of Maharashtra (2011)), approximately 1 million people would experience increased heat stress in this scenario. In relative terms, Cheng and McColl (2024b) used simple geometric arguments to show that, for square-shaped LRM schemes smaller than about 5 km × 5 km, more people would experience increases in warming (in the LRM scheme's immediate surroundings) than decreases (inside the LRM region). The same arguments apply here for wet-bulb temperatures and heat stress in sufficiently humid climates.

Finally, as discussed in Cheng and McColl (2024b), if LRM is primarily deployed in wealthier neighborhoods, the mechanism identified here will exacerbate existing heat inequality (Chakraborty et al., 2023). Our study shows that this effect extends to wet-bulb temperatures and heat stress in sufficiently humid climates.

Hot and humid regions are at imminent risk of severe heat stress (e.g., South Asia (Im et al., 2017) and the Persian/Arabian Gulf (Raymond et al., 2020)), and may seem like natural candidates for LRM. However, our study shows that deploying LRM in hot and humid regions may cause serious side-effects that, without mitigation, could well outweigh its potential benefits.

Conflict of Interest

The authors declare no conflicts of interest relevant to this study.

Availability Statement

The data set used for this study is publicly-available on the Harvard Dataverse (Cheng & McColl, 2024a).

Acknowledgments
We thank Marat Khairoutdinov for providing SAM and the land model SLM. The computations in this paper were run on the FASRC Cannon cluster supported by the FAS Division of Science Research Computing Group at Harvard University. K.A.M. acknowledges funding from NSF grant AGS-2129576, an NSF CAREER award (AGS-2441565), and a Sloan Research Fellowship (FG-2023-19963).

References

Abbott, T. H., & Cronin, T. W. (2021). Aerosol invigoration of atmospheric convection through increases in humidity. *Science*, *371*(6524), 83–85. https://doi.org/10.1126/science.abc5181

Alves de Oliveira, B. F., Bottino, M. J., Nobre, P., & Nobre, C. A. (2021). Deforestation and climate change are projected to increase heat stress risk in the Brazilian Amazon. *Communications Earth & Environment*, *2*(1), 207. https://doi.org/10.1038/s43247-021-00275-8

Betts, A. K. (2000). Idealized model for equilibrium boundary layer over land. *Journal of Hydrometeorology*, *1*(6), 507–523. https://doi.org/10.1175/1525-7541(2000)001<0507:IMFEBL>2.0.CO;2

Braghiere, R. K., Wang, Y., Gagné-Landmann, A., Brodrick, P. G., Bloom, A. A., Norton, A. J., et al. (2023). The importance of hyperspectral soil albedo information for improving Earth system model projections. *AGU Advances*, *4*(4), e2023AV000910. https://doi.org/10.1029/2023AV000910

Budd, G. M. (2008). Wet-bulb globe temperature (WBGT)—Its history and its limitations. *Journal of Science and Medicine in Sport*, *11*(1), 20–32. https://doi.org/10.1016/j.jsams.2007.07.003

Buzan, J. R., & Huber, M. (2020). Moist heat stress on a hotter Earth. *Annual Review of Earth and Planetary Sciences*, *48*(1), 623–655. https://doi.org/10.1146/annurev-earth-053018-060100

Chagnaud, G., Taylor, C. M., Jackson, L. S., Birch, C., Marsham, J., & Klein, C. (2025). Wet-bulb temperature extremes locally amplified by wet soils. *Geophysical Research Letters*, *52*(8), e2024GL112467. https://doi.org/10.1029/2024GL112467

Chakraborty, T., Newman, A. J., Qian, Y., Hsu, A., & Sheriff, G. (2023). Residential segregation and outdoor urban moist heat stress disparities in the United States. *One Earth*, *6*(6), 738–750. https://doi.org/10.1016/j.oneear.2023.05.016

Cheng, Y., Hu, Z., & McColl, K. A. (2023). Anomalously darker land surfaces become wetter due to mesoscale circulations. *Geophysical Research Letters*, *50*(17), e2023GL104137. https://doi.org/10.1029/2023GL104137

Cheng, Y., & McColl, K. (2024a). Replication data for: Unexpected warming from land radiative management (version V1). *Harvard Dataverse*. [Dataset]. https://doi.org/10.7910/DVN/ZEGHDW

Cheng, Y., & McColl, K. A. (2023). Thermally direct mesoscale circulations caused by land surface roughness anomalies. *Geophysical Research Letters*, *50*(16), e2023GL105150. https://doi.org/10.1029/2023GL105150

Cheng, Y., & McColl, K. A. (2024b). Unexpected warming from land radiative management. *Geophysical Research Letters*, *51*(22), e2024GL112433. https://doi.org/10.1029/2024GL112433

Dagan, G., & Stier, P. (2020). Constraint on precipitation response to climate change by combination of atmospheric energy and water budgets. *npj Climate and Atmospheric Science*, *3*(1), 34. https://doi.org/10.1038/s41612-020-00137-8

Davin, E. L., Seneviratne, S. I., Ciais, P., Olioso, A., & Wang, T. (2014). Preferential cooling of hot extremes from cropland albedo management. *Proceedings of the National Academy of Sciences of the United States of America*, *111*(27), 9757–9761. https://doi.org/10.1073/pnas.1317323111

Erell, E., Pearlmutter, D., Boneh, D., & Kutiel, P. B. (2014). Effect of high-albedo materials on pedestrian heat stress in urban street canyons. *Urban Climate*, *10*, 367–386. https://doi.org/10.1016/j.uclim.2013.10.005

Fan, Y., & McColl, K. A. (2024). Widespread outdoor exposure to uncompensable heat stress with warming. *Communications Earth & Environment*, *5*(1), 1–13. https://doi.org/10.1038/s43247-024-01930-6

Freychet, N., Hegerl, G. C., Lord, N. S., Lo, Y. E., Mitchell, D., & Collins, M. (2022). Robust increase in population exposure to heat stress with increasing global warming. *Environmental Research Letters*, *17*(6), 064049. https://doi.org/10.1088/1748-9326/ac71b9

Government of Maharashtra. (2011). Demography: Mumbai suburban district. Retrieved from https://mumbaisuburban.gov.in/en/demography/

Im, E.-S., Pal, J. S., & Eltahir, E. A. (2017). Deadly heat waves projected in the densely populated agricultural regions of south Asia. *Science Advances*, *3*(8), e1603322. https://doi.org/10.1126/sciadv.1603322

Irvine, P. J., Ridgwell, A., & Lunt, D. J. (2011). Climatic effects of surface albedo geoengineering. *Journal of Geophysical Research*, *116*(D24). https://doi.org/10.1029/2011JD016281

Jia, G., Shevliakova, E., Artaxo, P., De Noblet-Ducoudré, N., Houghton, R., House, J., et al. (Eds.), Climate change and land: An IPCC special report on climate change, desertification, land degradation, sustainable land management, food security, and greenhouse gas fluxes in terrestrial ecosystems. Cambridge Univ. Press. https://doi.org/10.1017/9781009157988.004

Khairoutdinov, M. F., & Randall, D. A. (2003). Cloud resolving modeling of the ARM summer 1997 IOP: Model formulation, results, uncertainties, and sensitivities. *Journal of the Atmospheric Sciences*, *60*(4), 607–625. https://doi.org/10.1175/1520-0469(2003)060<0607:CRMOTA>2.0.CO;2

Kiehl, J., Hack, J., Bonan, G., Boville, B., Williamson, D., & Rasch, P. (1998). The National Center for Atmospheric Research Community Climate Model: CCM3. *Journal of Climate*, *11*(6), 1131–1149. https://doi.org/10.1175/1520-0442(1998)011<1131:TNCFAR>2.0.CO;2

Kong, Q., & Huber, M. (2023). Regimes of soil moisture–wet-bulb temperature coupling with relevance to moist heat stress. *Journal of Climate*, *36*(22), 7925–7942. https://doi.org/10.1175/JCLI-D-23-0132.1

Krakauer, N. Y., Cook, B. I., & Puma, M. J. (2020). Effect of irrigation on humid heat extremes. *Environmental Research Letters*, *15*(9), 094010. https://doi.org/10.1088/1748-9326/ab9ecf

Lee, J. M., & Khairoutdinov, M. (2015). A Simplified Land Model (SLM) for use in cloud-resolving models: Formulation and evaluation. *Journal of Advances in Modeling Earth Systems*, *7*(3), 1368–1392. https://doi.org/10.1002/2014MS000419

Lee, X. (2018). *Fundamentals of boundary-layer meteorology* (Vol. 256). Springer.

Li, D., Bou-Zeid, E., & Oppenheimer, M. (2014). The effectiveness of cool and green roofs as urban heat island mitigation strategies. *Environmental Research Letters*, *9*(5), 055002. https://doi.org/10.1088/1748-9326/9/5/055002

Mackey, C. W., Lee, X., & Smith, R. B. (2012). Remotely sensing the cooling effects of city scale efforts to reduce urban heat island. *Building and Environment*, *49*, 348–358. https://doi.org/10.1016/j.buildenv.2011.08.004

Manabe, S., & Strickler, R. F. (1964). Thermal equilibrium of the atmosphere with a convective adjustment. *Journal of the Atmospheric Sciences*, *21*(4), 361–385. https://doi.org/10.1175/1520-0469(1964)021<0361:TEOTAW>2.0.CO;2

Manabe, S., & Wetherald, R. T. (1967). Thermal equilibrium of the atmosphere with a given distribution of relative humidity. *Journal of the Atmospheric Sciences*, *24*(3), 241–259. https://doi.org/10.1175/1520-0469(1967)024<0241:TEOTAW>2.0.CO;2

Matthews, A., McColl, K. A., & Kuang, Z. (2026). Bulk radiative-convective equilibrium is common over mid-latitude land. *Geophysical Research Letters*, *53*(4), e2025GL119923. https://doi.org/10.1029/2025GL119923

McColl, K. A., & Rigden, A. J. (2020). Emergent simplicity of continental evapotranspiration. *Geophysical Research Letters*, *47*(6), e2020GL087101. https://doi.org/10.1029/2020GL087101

McColl, K. A., & Tang, L. I. (2024). An analytic theory of near-surface relative humidity over land. *Journal of Climate*, *37*(4), 1213–1230. https://doi.org/10.1175/JCLI-D-23-0342.1

Miyawaki, O., Shaw, T. A., & Jansen, M. F. (2022). Quantifying energy balance regimes in the modern climate, their link to lapse rate regimes, and their response to warming. *Journal of Climate*, *35*(3), 1045–1061. https://doi.org/10.1175/JCLI-D-21-0440.1

Pal, J. S., & Eltahir, E. A. (2016). Future temperature in southwest Asia projected to exceed a threshold for human adaptability. *Nature Climate Change*, *6*(2), 197–200. https://doi.org/10.1038/nclimate2833

Powis, C. M., Byrne, D., Zobel, Z., Gassert, K. N., Lute, A., & Schwalm, C. R. (2023). Observational and model evidence together support widespread exposure to noncompensable heat under continued global warming. *Science Advances*, *9*(36), eadg9297. https://doi.org/10.1126/sciadv.adg9297

Raymond, C., Matthews, T., & Horton, R. M. (2020). The emergence of heat and humidity too severe for human tolerance. *Science Advances*, *6*(19), eaaw1838. https://doi.org/10.1126/sciadv.aaw1838

Saeed, F., Schleussner, C.-F., & Ashfaq, M. (2021). Deadly heat stress to become commonplace across south Asia already at 1.5 C of global warming. *Geophysical Research Letters*, *48*(7), e2020GL091191. https://doi.org/10.1029/2020GL091191

Safieddine, S., Clerbaux, C., Clarisse, L., Whitburn, S., & Eltahir, E. A. (2022). Present and future land surface and wet bulb temperatures in the Arabian peninsula. *Environmental Research Letters*, *17*(4), 044029. https://doi.org/10.1088/1748-9326/ac507c

10.1029/2026GL125630

Seneviratne, S. I., Corti, T., Davin, E. L., Hirschi, M., Jaeger, E. B., Lehner, I., et al. (2010). Investigating soil moisture–climate interactions in a changing climate: A review. *Earth-Science Reviews*, *99*(3–4), 125–161. https://doi.org/10.1016/j.earscirev.2010.02.004

Seneviratne, S. I., Phipps, S. J., Pitman, A. J., Hirsch, A. L., Davin, E. L., Donat, M. G., et al. (2018). Land radiative management as contributor to regional-scale climate adaptation and mitigation. *Nature Geoscience*, *11*(2), 88–96. https://doi.org/10.1038/s41561-017-0057-5

Sharma, A., Conry, P., Fernando, H., Hamlet, A. F., Hellmann, J., & Chen, F. (2016). Green and cool roofs to mitigate urban heat island effects in the Chicago metropolitan area: Evaluation with a regional climate model. *Environmental Research Letters*, *11*(6), 064004. https://doi.org/10.1088/1748-9326/11/6/064004

Sherwood, S. C., & Huber, M. (2010). An adaptability limit to climate change due to heat stress. *Proceedings of the National Academy of Sciences of the United States of America*, *107*(21), 9552–9555. https://doi.org/10.1073/pnas.0913352107

Sobel, A. H., Nilsson, J., & Polvani, L. M. (2001). The weak temperature gradient approximation and balanced tropical moisture waves. *Journal of the Atmospheric Sciences*, *58*(23), 3650–3665. https://doi.org/10.1175/1520-0469(2001)058<3650:TWTGAA>2.0.CO;2

Taleghani, M., Sailor, D., & Ban-Weiss, G. A. (2016). Micrometeorological simulations to predict the impacts of heat mitigation strategies on pedestrian thermal comfort in a Los Angeles neighborhood. *Environmental Research Letters*, *11*(2), 024003. https://doi.org/10.1088/1748-9326/11/2/024003

Vahmani, P., Sun, F., Hall, A., & Ban-Weiss, G. (2016). Investigating the climate impacts of urbanization and the potential for cool roofs to counter future climate change in southern California. *Environmental Research Letters*, *11*(12), 124027. https://doi.org/10.1088/1748-9326/11/12/124027

Van der Ent, R. J., Savenije, H. H., Schaefli, B., & Steele-Dunne, S. C. (2010). Origin and fate of atmospheric moisture over continents. *Water Resources Research*, *46*(9). https://doi.org/10.1029/2010WR009127

Vanos, J., Guzman-Echavarria, G., Baldwin, J. W., Bongers, C., Ebi, K. L., & Jay, O. (2023). A physiological approach for assessing human survivability and liveability to heat in a changing climate. *Nature Communications*, *14*(1), 7653. https://doi.org/10.1038/s41467-023-43121-5

Vecellio, D. J., Kong, Q., Kenney, W. L., & Huber, M. (2023). Greatly enhanced risk to humans as a consequence of empirically determined lower moist heat stress tolerance. *Proceedings of the National Academy of Sciences of the United States of America*, *120*(42), e2305427120. https://doi.org/10.1073/pnas.2305427120

Wang, J., Bras, R. L., & Eltahir, E. A. (2000). The impact of observed deforestation on the mesoscale distribution of rainfall and clouds in Amazonia. *Journal of Hydrometeorology*, *1*(3), 267–286. https://doi.org/10.1175/1525-7541(2000)001<0267:TIOODO>2.0.CO;2

Wilhelm, M., Davin, E. L., & Seneviratne, S. I. (2015). Climate engineering of vegetated land for hot extremes mitigation: An Earth system model sensitivity study. *J. Geophys. Res.-Atmos.*, *120*(7), 2612–2623. https://doi.org/10.1002/2014JD022293

Wouters, H., Keune, J., Petrova, I. Y., Van Heerwaarden, C. C., Teuling, A. J., Pal, J. S., et al. (2022). Soil drought can mitigate deadly heat stress thanks to a reduction of air humidity. *Science Advances*, *8*(1), eabe6653. https://doi.org/10.1126/sciadv.abe6653

Yang, B., Yang, X., Leung, L. R., Zhong, S., Qian, Y., Zhao, C., et al. (2019). Modeling the impacts of urbanization on summer thermal comfort: The role of urban land use and anthropogenic heat. *Journal of Geophysical Research: Atmospheres*, *124*(13), 6681–6697. https://doi.org/10.1029/2018JD029829

Zhang, K., Cao, C., Chu, H., Zhao, L., Zhao, J., & Lee, X. (2023). Increased heat risk in wet climate induced by urban humid heat. *Nature*, *617*(7962), 738–742. https://doi.org/10.1038/s41586-023-05911-1

Supporting Information for Land radiative management increases heat stress in some humid regions

Yu Cheng[1,2], Kaighin A. McColl[2,3]

[1]Shanghai Key Laboratory of Ocean-land-atmosphere Boundary Dynamics and Climate Change, Department of Atmospheric and Oceanic Sciences, Fudan University, Shanghai, China
[2]Department of Earth and Planetary Sciences, Harvard University, Cambridge, Massachusetts, USA
[3]School of Engineering and Applied Sciences, Harvard University, Cambridge, Massachusetts, USA

Contents of this file

Figs. S1 to S11

Tables S1 & S2

Corresponding author: Kaighin A. McColl, kmccoll@seas.harvard.edu

Table S1. Modelling experiments performed in this study. τ denotes simulation length and Δx denotes horizontal resolution. "LRM visible albedo" and "Background visible albedo" indicate visible dry surface albedos in and around the LRM region, respectively."LRM near-infrared (NIR) albedo" and "Background near-infrared (NIR) albedo" indicate near-infrared dry surface albedos in and around the LRM region, respectively. Actual surface albedos respond to soil saturation in our simulations. "Domain" indicates domain geometry used (Fig. S1). "Large scale forcing?" indicates which approximation was used for atmospheric dynamics: radiative-convective equilibrium (RCE) or the weak temperature gradient approximation (WTG). "Mean wind?" indicates simulations for which a mean wind of $U = 10$ m s^{-1} was prescribed ('Y') or not prescribed ('N').

Experiment name	τ (days)	Δx (m)	LRM visible albedo	LRM near-infrared (NIR) albedo	Background visible albedo	Background near-infrared (NIR) albedo	Domain	Large scale forcing	Mean wind?
A_RCE	1000	1000	0.19	0.38	0.0475	0.095	A	RCE	N
A_RCE_nudgesoil	1000	1000	0.19	0.38	0.0475	0.095	A	RCE	N
A_RCE_wind	1000	1000	0.19	0.38	0.0475	0.095	A	RCE	Y
A_RCE_grassland	1000	1000	0.5	0.5	0.19	0.38	A	RCE	N
A_RCE_urban	1000	1000	0.5	0.5	0.19	0.38	A	RCE	N
A_WTG	796	1000	0.19	0.38	0.0475	0.095	A	WTG	N
B_WTG	1033	250	0.19	0.38	0.0475	0.095	B	WTG	N
C_RCE	1000	1000	0.19	0.38	0.0475	0.095	C	RCE	N

Table S2. Summary of simulated climates for each modelling experiment. All quantities are daytime-averaged (6 a.m.–6 p.m.) over land. "TOA insolation" is top-of-atmosphere insolation.

Numerical experiments	Daytime-averaged TOA insolation (W m^{-2})	$\overline{\langle s \rangle}$	$\overline{\langle RH \rangle}$	$\overline{\langle T_a \rangle}$ (°C)	$\overline{\langle T_w \rangle}$ (°C)
A_RCE	546	0.16	51%	41	32
	535	0.19	64%	35	30
	524	0.22	69%	32	27
	514	0.24	72%	29	25
	452	0.35	86%	14	12
	438	0.37	84%	11	9
A_RCE_nudgesoil	548	0.27	77%	38	34
	539	0.28	78%	35	31
	531	0.28	78%	33	29
	523	0.29	77%	30	27
A_RCE_wind	462	0.35	80%	15	13
A_RCE_grassland	396	0.48	87%	9	8
A_RCE_urban	417	0.39	83%	6	5
A_WTG	508	0.72	86%	27	25
B_WTG	530	0.50	87%	26	24
C_RCE	488	0.61	83%	18	16

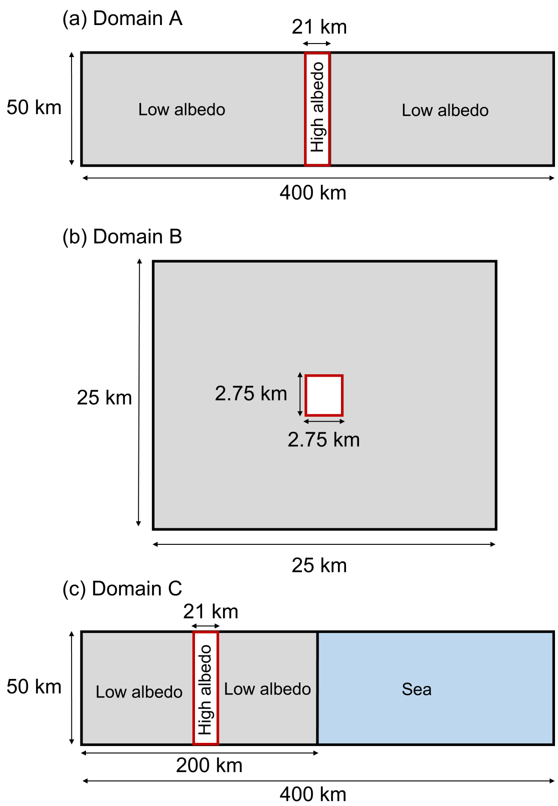

Figure S1. Modelling geometries (not to scale).

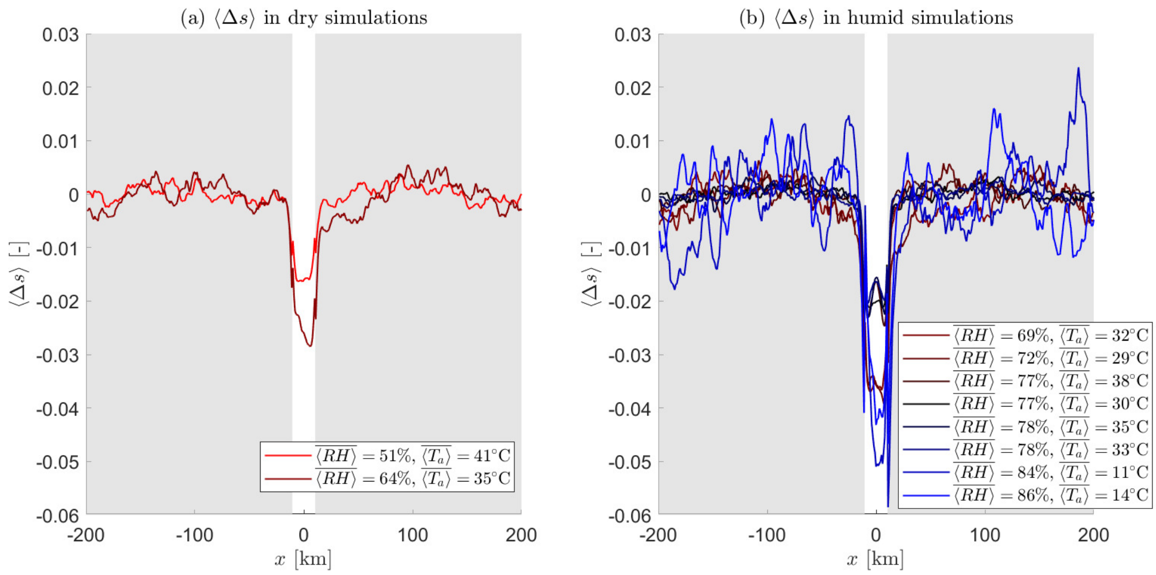

Figure S2. Same as Fig. 1, but for soil saturation s.

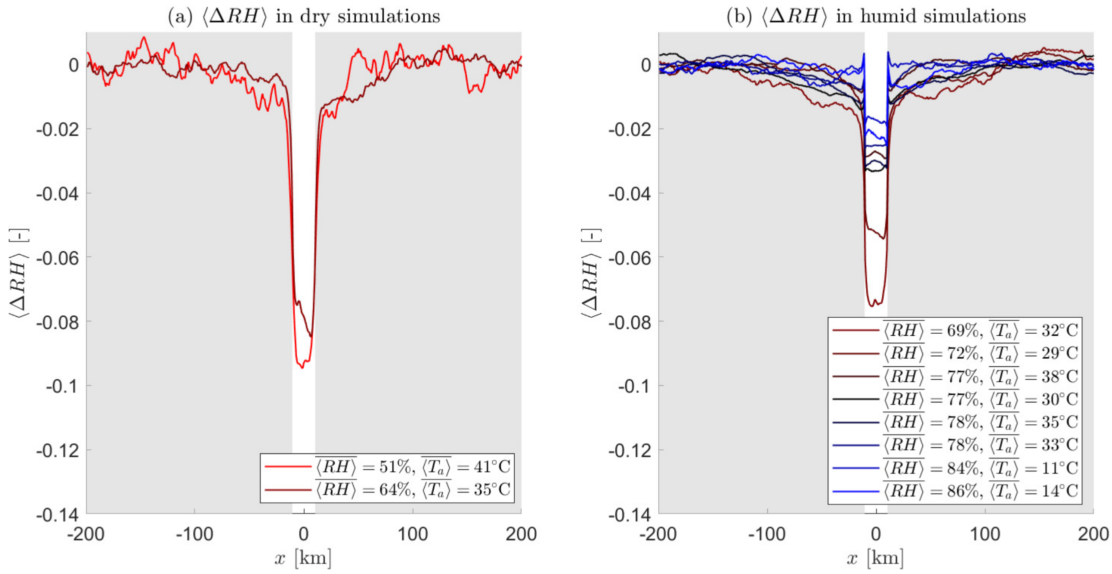

Figure S3. Same as Fig. 1, but for relative humidity RH.

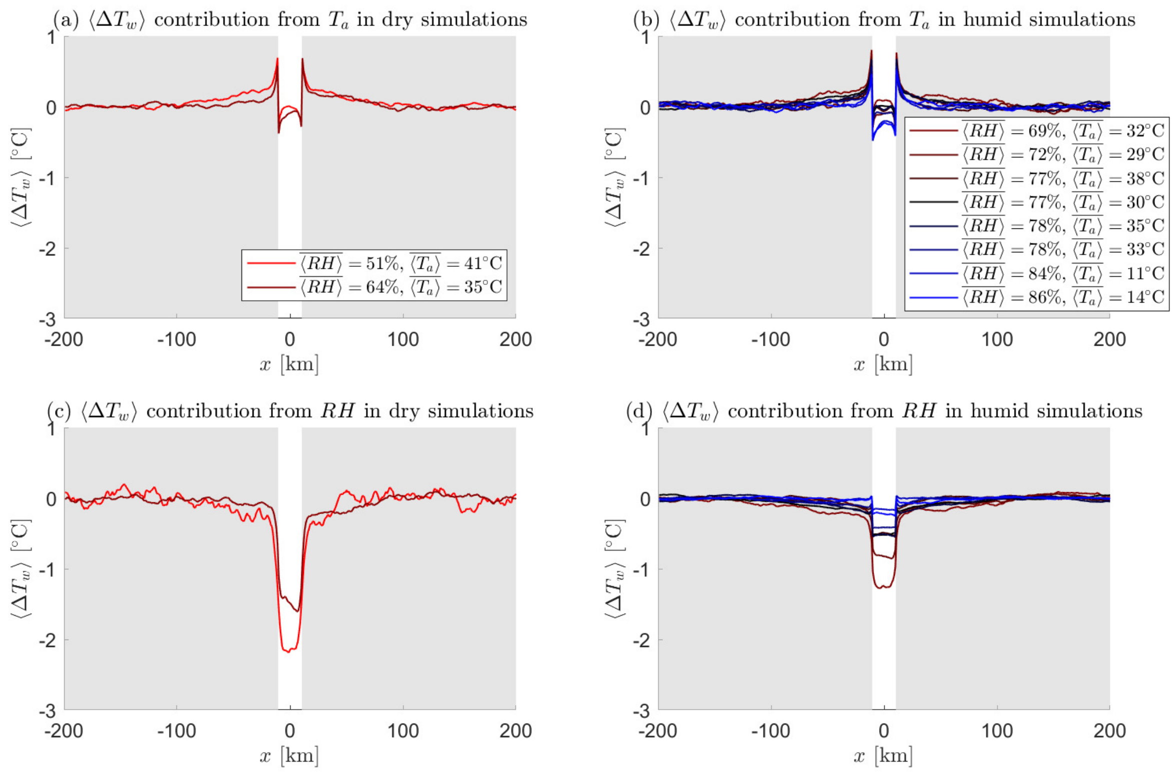

Figure S4. Same as Fig. 1, but for (a) & (b) contributions from T_a to ΔT_w; and (c) & (d) contributions from RH to ΔT_w. The decomposition of $\langle \Delta T_w \rangle$ is based on Equation 3.

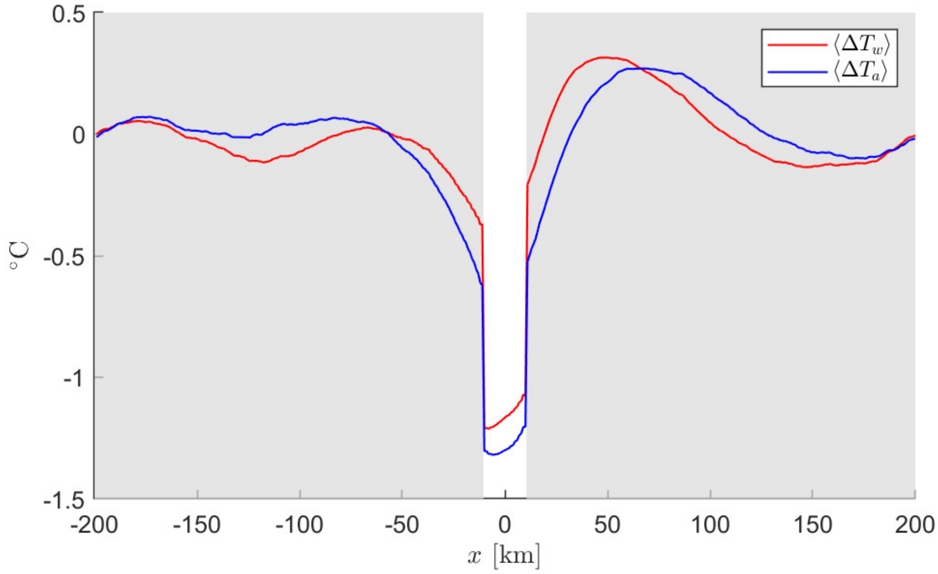

Figure S5. Near-surface wet-bulb temperature ($\langle \Delta T_w \rangle$) and near-surface air temperature ($\langle \Delta T_a \rangle$) anomalies in A_RCE_wind. The results are not partitioned between dry and humid simulations because only one simulation was conducted (Table S1), corresponding to a humid climate (Table S2).

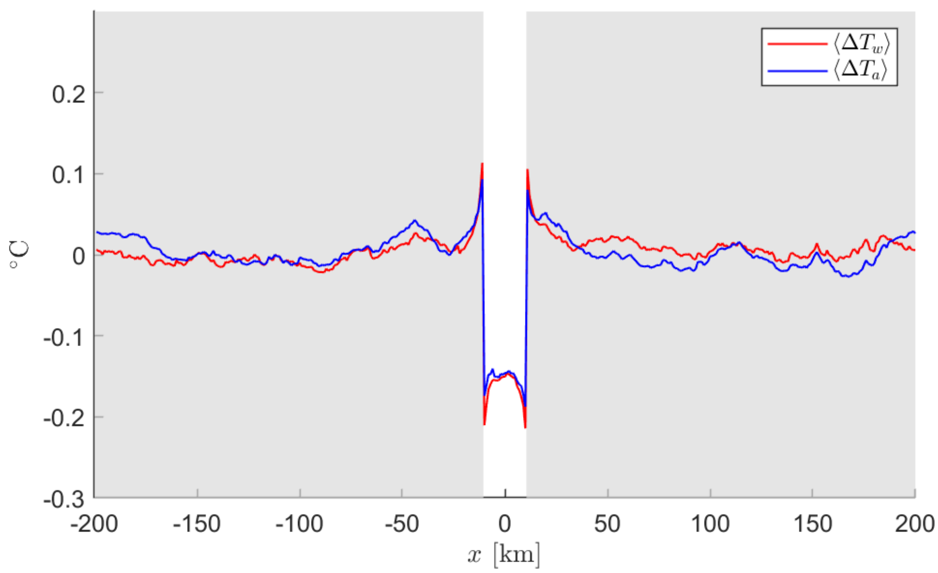

Figure S6. Same as Fig. S5 but for the simulation A_WTG (Table S1).

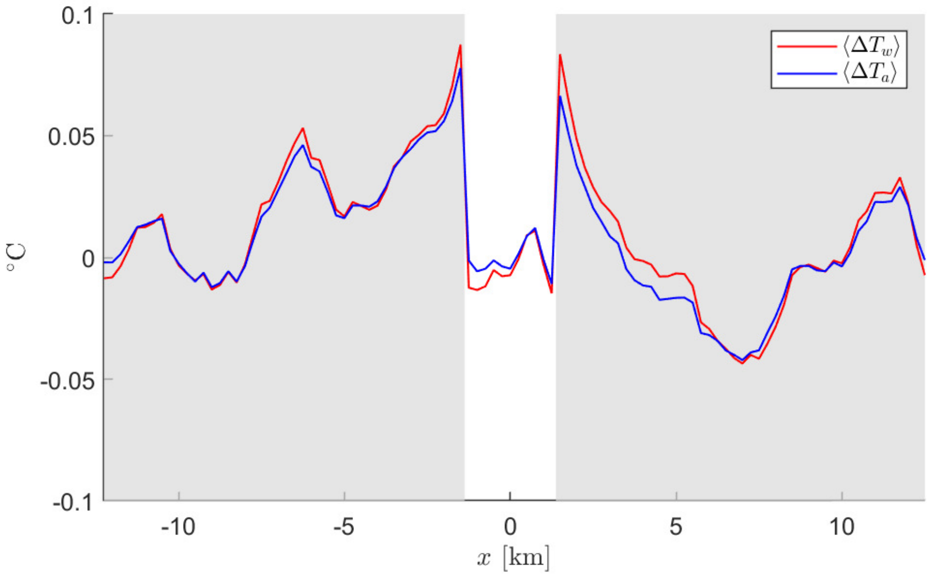

Figure S7. Same as Fig. S5 but for the simulation B_WTG (Table S1).

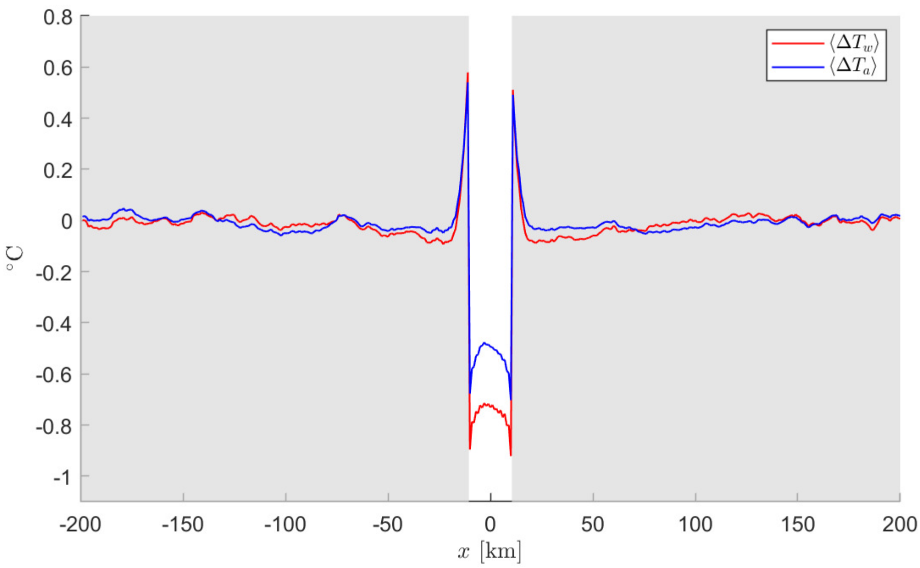

Figure S8. Same as Fig. S5 but for the simulation A_RCE_grassland.

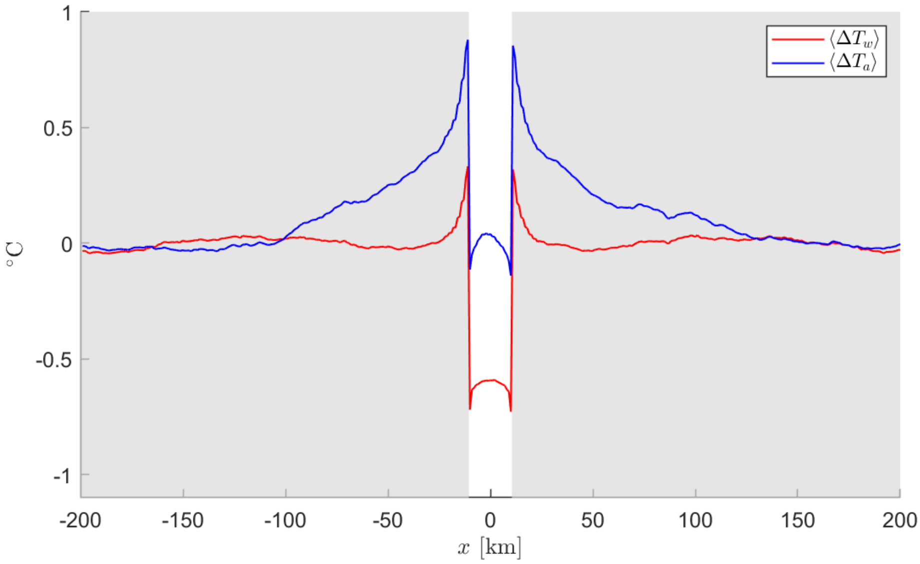

Figure S9. Same as Fig. S5 but for the simulation A_RCE_urban.

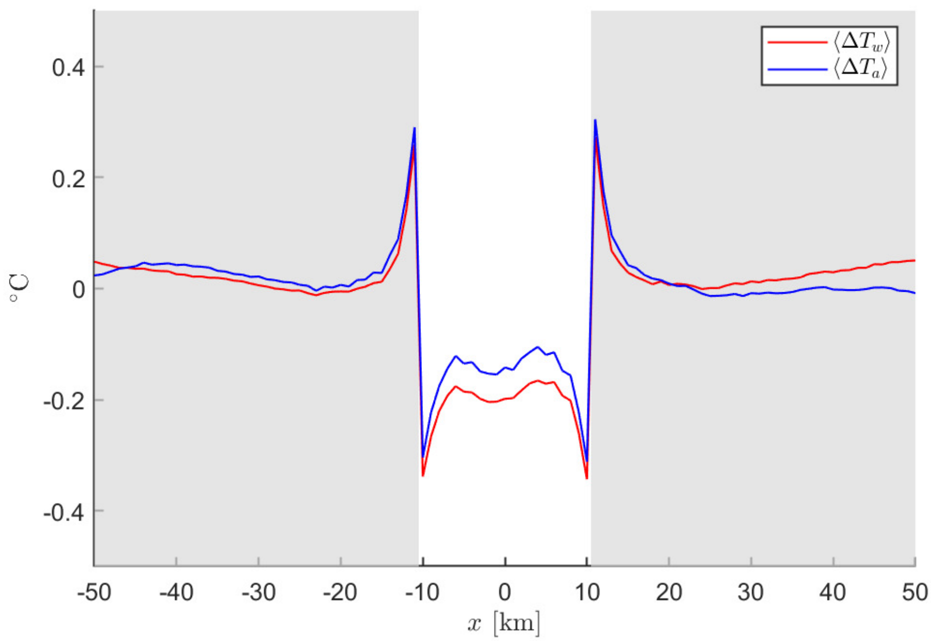

Figure S10. Same as Fig. S5 but for the simulation C_RCE. The x-axis length of the domain is smaller than in Fig. S5 because, in this simulation, one half of the surface is land and the other half is sea.

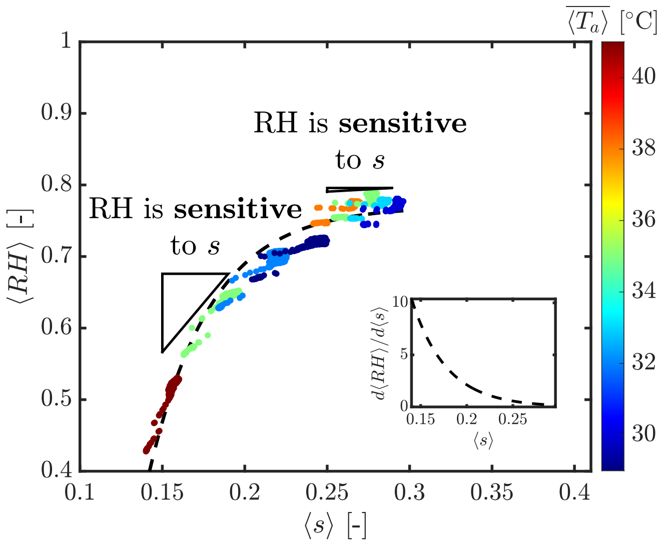

Figure S11. Same as Fig. 3 but with colder simulations ($\overline{\langle T_a \rangle} < 20°C$) removed, and with the colorbar adjusted accordingly.